Journal of Superconductivity and Novel Magnetism (2025) 38:89
https://doi.org/10.1007/s10948-025-06933-8

RESEARCH

X-Ray Computed Tomography Study of the Microstructure of Superconducting MgB_2 Bulks

Yingqing Wang[1] · Chris Grovenor[2] · Susannah Speller[2] · Barbara Shollock[1] · Tayebeh Mousavi[1]

Received: 5 December 2024 / Accepted: 10 February 2025

Abstract
MgB_2 is a promising candidate for commercial superconducting applications because, as grain boundaries in MgB_2 are not weak links, there are fewer limitations on the choice of processing technique compared to high-temperature superconducting (HTS) cuprates. MgB_2 bulks are usually manufactured by powder processing techniques followed by a sintering process. After sintering, the impurity phases such as MgO and MgB_4 along with porosity are formed which strongly affect the superconducting properties mainly the macroscopic path for supercurrent in MgB_2 bulks. Investigation of these microstructural features is essential to improve the superconducting properties of these bulks. In this work, high-resolution laboratory X-ray computed tomography (XCT) has been used to investigate the microstructure of MgB_2 bulks in three dimensions. The volume fraction of defects and impurity phases along with the size distribution of pores have been studied using this advanced technique. A comparison has been made between the data extracted from conventional characterization techniques such as XRD and SEM and those obtained from the advanced XCT analysis.

Keywords Superconducting bulks · X-ray computed tomography · 3D analysis

1 Introduction

MgB_2 is considered a promising material in the field of applied superconductivity due to its relatively high critical temperature of 39 K (Tc) which makes it suitable for liquid helium-free applications, in contrast to conventional low-temperature superconductors (LTSs) such as NbTi and Nb_3Sn [1–4]. Moreover, MgB_2 can be manufactured in bulk by scalable and readily available powder metallurgy routes which are much easier and cheaper compared to those processing techniques used for high-temperature superconductor (HTS) materials such as cuprates [5–8]. In addition, MgB_2 does not contain any rare earth or toxic elements that usually exist in HTS [9, 10]. This combination of properties makes MgB_2 an attractive candidate to replace 'traditional' LTS materials such as NbTi in applications including MRI machines and magnetic drug targeting devices [1, 11, 12].

The main manufacturing technique for MgB_2 bulks involves a standard powder processing process followed by a heat treatment [13]. This processing technique can be carried out either in-situ or ex-situ [14]. In the in-situ process, Mg and B precursor powders react together to form the MgB_2 phase at moderate temperatures (less than 900 °C) during the heat treatment. In the case of the ex-situ route, pre-synthesised MgB_2 powder is consolidated at high temperatures (above 900 °C), usually with the assistance of pressure to achieve densification.

The research carried out for MgB_2 bulks and wires showed that heating under high isostatic pressure allows for a significant increase in the density of the MgB_2, and improves its homogeneity, improves inter-grain connections, reduces voids, and increases critical parameters [15–18]. Moreover, the density of the untreated MgB_2 material before the synthesis reaction significantly affects the formation of the MgB_2 superconducting phase [19–21]. In all of these synthesis processes, dopants also play a significant role in both the manufacturing process and final superconducting properties [22].

The MgB_2 bulks manufactured by powder processing techniques usually include impurity phases, mainly MgO and MgB_4, as well as porosity and gaps between the grains

✉ Tayebeh Mousavi
tayebeh.mousavi@kcl.ac.uk

[1] Department of Engineering, King's College London, London WC2R 2LS, UK

[2] Department of Materials, University of Oxford, Oxford OX1 3PH, UK

Published online: 18 February 2025

which limit the cross-sectional area for supercurrent transport [23]. MgB_4 forms by the thermal decomposition of MgB_2, and the porosity is usually formed as a result of the sintering process of a brittle material, and the impurity phases are usually formed as a result of high-temperature sintering process [24]. Since these microstructural features strongly affect the critical current of the MgB_2 bulk, the main challenge is how to improve the density and connectivity of MgB_2 bulks without using high temperatures that promote the formation of impurities and increase the manufacturing cost.

However, these microstructural features need to be investigated carefully in MgB_2 bulks in order to make a precise correlation between processing parameters and microstructure, and finally to optimize the processing techniques to achieve MgB_2 bulks with minimized porosity and large impurity phase particles. The impurity and porosity of MgB_2 bulks have been widely investigated in the literature [25]. In most of these studies, different types of electron microscopy have been used to investigate the microstructure. While all these techniques are well established as powerful tools in the characterization of materials, they rely on 2D images where the information in one dimension is always missing in the analysis.

This work focuses on using a new advanced characterization technique, X-ray computed tomography (XCT), to look at the microstructure of MgB_2 bulks in three dimensions rather than conventional two-dimensional techniques. XCT is a relatively novel method for 3D microstructure characterization of bulk materials, using synchrotron or laboratory X-ray microscopes [26]. Compared with conventional 2D characterization methods, XCT can provide accurate and high-resolution 3D observations of the microstructure, while avoiding the possible introduction of manual damage during the sample preparation process. Consequently, XCT as an advanced non-destructive technique has been applied to a range of materials to look at various microstructural features such as porosity [27–30]. This study is focused on using this advanced technique to examine the microstructure of MgB_2 bulks in 3D. The results present 3D visualization of various features in MgB_2 bulks and provide information on the volume fraction of impurities and porosity along with the size distribution of these features. Conventional techniques including scanning electron microscopy (SEM) and X-ray diffraction (XRD) were also used to investigate the samples. Finally, a comparison was made between the results of the 3D analysis by XCT and those of the 2D analysis by conventional techniques.

2 Methodology

2.1 MgB_2 Fabrication

MgB_2 bulk samples were fabricated from commercial MgB_2 powders (purity: 99%, size < 10 µm, Alfa Aesar) and a sintering process. The MgB_2 powders were placed into a graphite die protected with graphite paper. Two graphite punches were used to complete the assembly. The powder was sintered through cold pressing followed by a hot pressing process using spark plasma sintering (SPS). It was first compacted at room temperature in the graphite die using a uni-axial press at a pressure of 30 MPa for 1 min. The die assembly was then transferred into a Dr Fritsch DSP 507 FAST apparatus operating with a constant voltage and pulsed current ranging between 1.5–4 V and 0.4–1.2 kA. Before sintering, the chamber was evacuated and filled with Ar a few times to make an oxygen-free chamber by removing any residual oxygen. The sintering chamber was then continuously evacuated during the sintering process to reach a baseline pressure of approximately 0.4–0.6 mbar. The samples were heated from room temperature to 900 °C at a rate of 100 °C /min and maintained at this temperature for 10 min (Sample 1) and 20 min (Sample 2). Then the pressure was gradually increased to 40 MPa (Sample 1) and 30 MPa (Sample 2). Finally, the samples were maintained for about 5 min at 900 °C, before being progressively released during the final cooling step. The density of the MgB_2 bulk before and after this sintering process was measured to be 2.1 g cm^{-3} and 2.45 g cm^{-3} respectively.

2.2 Characterization

The MgB_2 bulk samples were characterized using different techniques including conventional x-ray diffraction (XRD) and scanning electron microscopy (SEM) techniques and advanced X-ray computed tomography (XCT) facility.

The SEM analysis was carried out using a JEOL 5510 SEM with OI SDD detector operating at 20 kV accelerating voltage. Higher spatial-resolution chemical analysis was performed using a Zeiss Merlin SEM with an Oxford Instruments 150 mm^2 XMax EDX detector. The phase fraction of each phase was calculated from the SEM images using image processing techniques.

The XRD measurements were carried out in a Rigaku Miniflex diffractometer using Cukα radiation ($\lambda = 0.154$ nm) at 40 kV and 15 mA. The weight fraction of the different phases detected in the bulk specimens were estimated from the XRD data by using Rietveld refinement (PANalytical HighScore Plus software) using the Hill and Howard method [31].

The tomographic imaging was performed using an Xradia Versa 510 X-ray microscope at Oxford University. The MgB_2 samples were cut to a size of 1 mm in cross-section in order to be firmly secured to the sample holder and thus to minimize sample movement during image acquisition. For each scan, 2000 radiographs, each with an exposure time of 10 s, was taken over a 360-degree rotation. The tomography was reconstructed using the microscope software. The volume analysed was approximately 980_980_200 voxels with a resolution of 0.561 µm per voxel side (i.e. ~0.55 mm×0.55 mm×0.12 mm).

3 Results and Discussion

3.1 XCT Results

3.1.1 Image Processing

The XCT data was analyzed using ImageJ and Avizo software. For precise analysis including the phase segmentation carried out using the Avizo software, the XCT images were first modified in ImageJ mainly for clear contrast between different phases and voids. 2D slice images after processing are shown in Fig. 1 for Sample 1 and Sample 2 at different magnifications. It can be seen that the images include features with different contrasts corresponding to different phases of MgB_2, MgB_4, MgO and voids. In XCT, different contrasts are due to phases with different x-ray absorption which will scale with atomic number. The MgB_2 matrix has light grey contrast, the MgB_4 phase is dark grey, the bright features are MgO, and the pores are usually black. For both samples, the 2D slices taken from different locations are relatively similar with almost the same features indicating that the samples manufactured in this work are macroscopically uniform.

3.1.2 Quantification and Data Analysis

To quantitatively analyse the phase fractions in the MgB_2 sample, Interactive Thresholding, a commonly used image segmentation module, was used to separately extract the voids and MgO phase from the background based on their contrast, i.e. different voxel grey levels. Interactive thresholding creates a binary image where the intensity level of 1 represents the features above the threshold, and 0 represents the background.

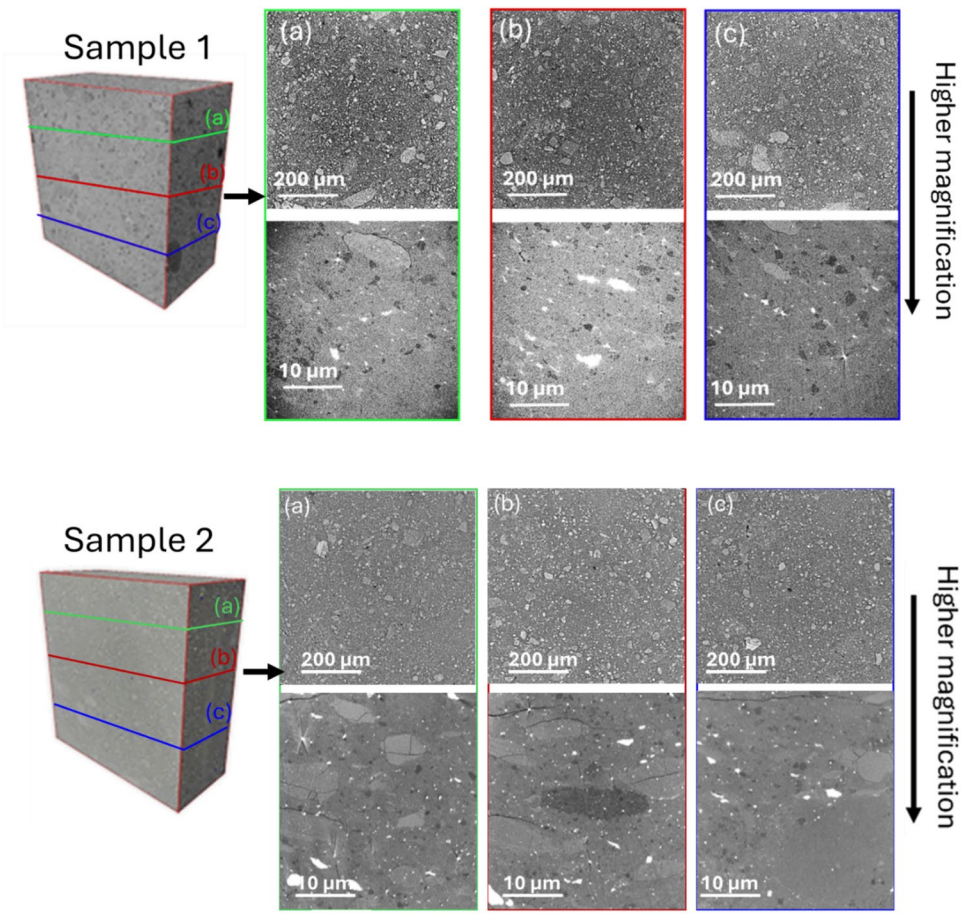

Fig. 1 2D virtual slices of MgB_2 bulk (Sample 1 and Sample 2) at different magnifications taken from different locations (a, b and c shown in the left image) by XCT

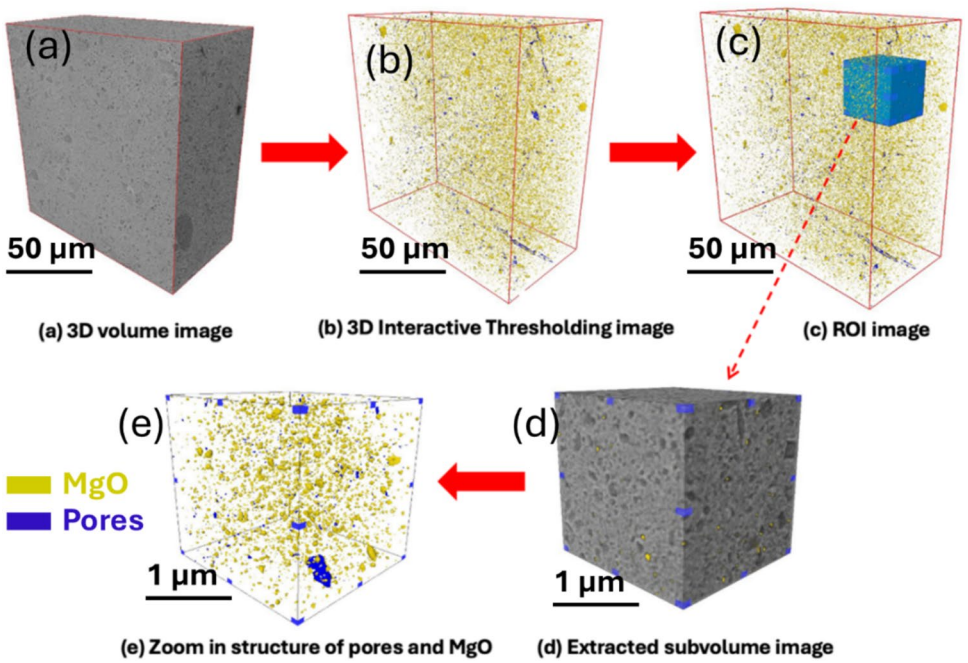

Fig. 2 Segmentation process of extracting interest sub-volume. **a** 3D visualization of the MgB_2 sample, (**b**) 3D visualization of MgO and pores after segmentation, (**c**-**e**) 3D visualization of the zoomed-in selected area

Figure 2a shows 3D visualization of the MgB_2 sample (sample 1) before segmentation, and Fig. 2b shows the 3D visualization of MgO (yellow colour) and pores (blue colour) in the MgB_2 sample after segmentation and applying the "Interactive Thresholding" function in Avizo. As can be seen, the MgO particles are evenly distributed within the MgB_2 matrix.

Figure 2c-e shows the 3D visualization of the same phases (MgO and voids) at higher magnification after applying "Interactive Thresholding", Region of Interest (ROI) and "Extract Volume" module functions in Avizo to zoom in specific sub-volume to present a clear view of the structure.

Figure 3 shows the 3D visualization of MgO and pores in two MgB_2 samples sintered under different conditions, as explained in Section 2.1. In both samples, the distribution of the MgO phase is relatively uniform across the entire sample. However, sample 1 includes a larger number of smaller MgO particles compared to sample 2 which consists of a smaller number of larger MgO particles. Sample 2 was maintained at a high temperature (900 °C) for a longer time (20 min) before applying the pressure compared to sample 1. This facilitates the oxidation of Mg as well as atomic diffusion in sample 2 leading to larger particles of MgO.

In contrast, sample 1 was maintained at a high temperature for a shorter time resulting in small MgO particles

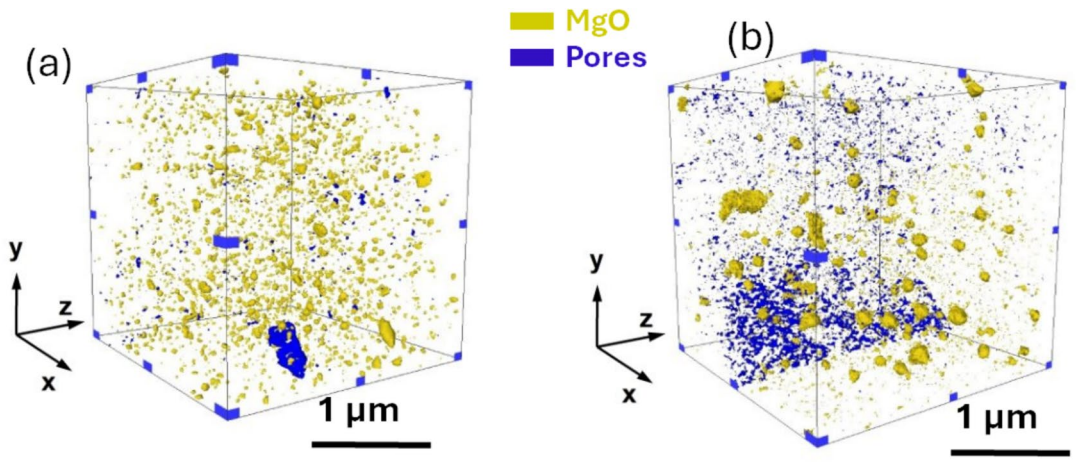

Fig. 3 3D visualizations of MgO phase and porosity in MgB_2 bulk samples (**a**) Sample 1 and (**b**) Sample 2. These 3D images were obtained by threshold segmentation of tomographs to remove the MgB_2 matrix and visualize the MgO and pores as explained in the text

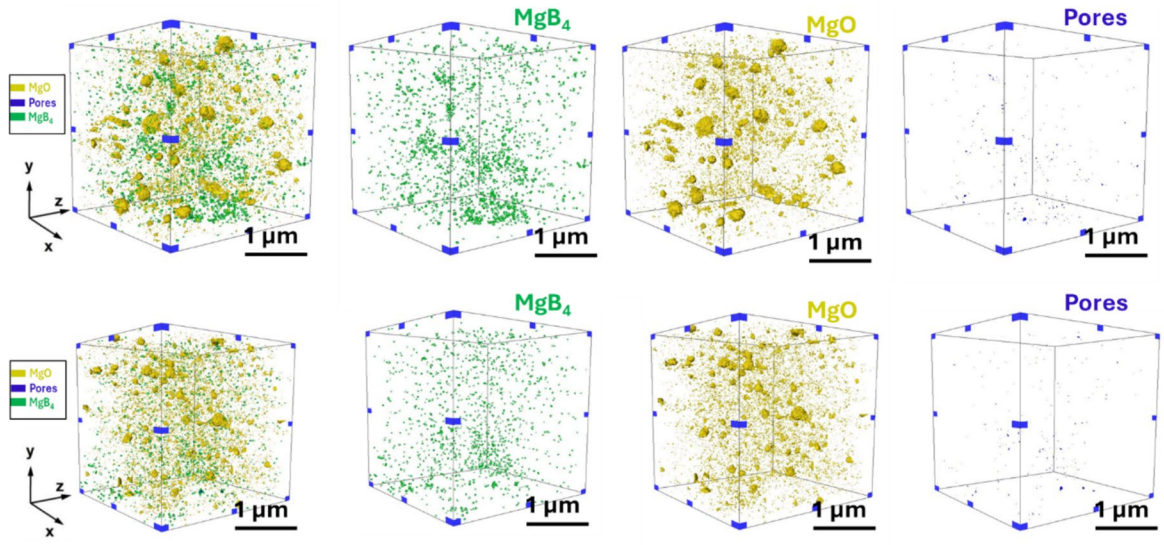

Fig. 4 3D visualizations of MgB_4, MgO and pores in the MgB_2 bulk sample using XCT technique

nucleating evenly across the sample with limited time to growth. Consequently, this sample includes smaller MgO particles distributed uniformly in the MgB_2 matrix. Interestingly, in contrast to MgO phase, the distribution of the pores is not uniform, especially in sample 2. Figure 4 shows the 3D visualization of MgB_4, MgO and pores in two different regions in Sample 2. As can be seen, the MgB_4 particles are much smaller compared to the MgO particles, however, the two regions show relatively similar distribution of the MgB_4 and MgO indicating that the MgB_2 bulk is macroscopically uniform. To quantitatively investigate these microstructural features, pores and MgO were separated with a "Separate Object" module before applying the equivalent diameter equation in the Label Analysis module to calculate the diameter of pores and solid particles. The segmented model was then further analyzed, and the resulting quantitative parameters were obtained as listed in Table 1. Sample 1 includes about 2 vol.% of porosity versus 3.5 vol.% of porosity for sample 2 indicating that sintering parameters for sample 1 including higher pressure and shorter time leads to a denser microstructure, desirable for superconducting applications. Moreover, although the size of the MgO particles is different, the MgO vol.% is almost similar for both samples. This is because the small MgO particles can join together making larger particles if they are given sufficient time at high temperatures. This is the case of the sintering parameters in sample 1.

3.2 SEM and XRD Characterization

Figure 5 shows the SEM images of MgB_2 samples. Sample 1 shows a well-connected microstructure containing a small volume fraction of pores (black regions). In contrast, sample 2 shows more porosity consistent with the XCT data presented in Table 1. At higher magnification, sample

Table 1 Quantitative parameters of pores and MgO particles calculated from the XCT data

	Pore diameter (μm) (±0.1)	MgO diameter (μm) (±0.1)	MgB_4 diameter (μm) (±0.1)	Vol.% pore (±0.04)	Vol.% MgO (±0.04)	Vol.% MgB_4 (±0.04)
Sample 1						
Minimum	0.008	0.08	0.009	2.1	8.23	4.1
Average	0.06	0.19	0.08			
Maximum	4.32	2.39	1.7			
Sample 2						
Minimum	0.007	0.09	0.01	3.5	8.18	4.8
Average	0.11	0.28	0.08			
Maximum	2.61	2.95	1.9			

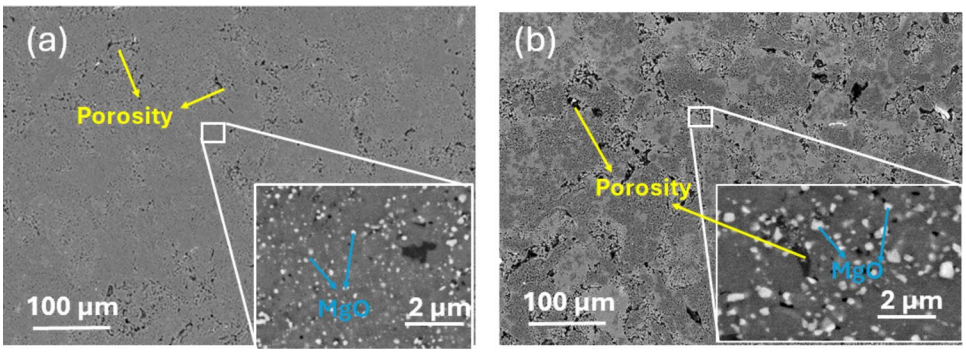

Fig. 5 The SEM images of MgB_2 bulk samples (**a**) sample 1, (**b**) sample 2

1 shows four different contrast levels corresponding to the solid phases of MgB_2 (light grey), MgB_4 (dark grey) and MgO (white), and porosity (black). This phase assignation has been confirmed by energy-dispersive X-ray elemental maps. This data shows that the MgB_2 bulk consists of a connected matrix of MgB_2 phase with fine round MgO particles (< 1 µm) and individual larger particles of MgB_4 randomly distributed over the matrix. Sample 2 shows larger MgO particles as well as more individual pores that can interrupt a continuous path for supercurrent.

The volume fraction of pores and MgO was calculated from the SEM images by dividing the number of pixels corresponding to these phases by the total number of pixels in the image. The results show that sample 1 includes 8 vol.% MgO and 2.3 vol.% pores whereas sample 2 consists of 8.7 vol.% MgO and 6.3 vol.% pores. Comparing this data with the volume fractions calculated from the XCT data, it can be seen that a relatively large difference exists for the volume fraction of pores when calculated by SEM and XCT (especially for sample 2). Looking at the 3D visualization of sample 2 at high magnification (Fig. 3b), the pores are not uniformly distributed over the sample. As a result, when the sample is analyzed by SEM, a 2D analysis technique, it is more likely that the SEM image is not representative of the entire sample leading to results that are less representative of the bulk.

Figure 6 shows the XRD patterns of MgB_2 bulks prepared at different sintering conditions (sample 1 and sample 2). The XRD peaks were identified as corresponding to MgO, MgB_2 and MgB_4 phases. No other phases were detected in the XRD data. This is consistent with the SEM and XCT data. The presence of MgB_4 and MgO impurity phases in MgB_2 bulks has been widely reported in the literature [32]. To quantify the fraction of each phase from XRD data, the XRD patterns were analysed by Rietveld refinement. The wt.% of MgO and MgB_4 were calculated to be 8.1 and 4.2 respectively for sample 1, and 9.5 and 4.8 respectively for sample 2. Consistent with the XCT data (Table 1), the fraction of MgO is relatively similar in both samples because of the reasons explained in Section 3.1.2.

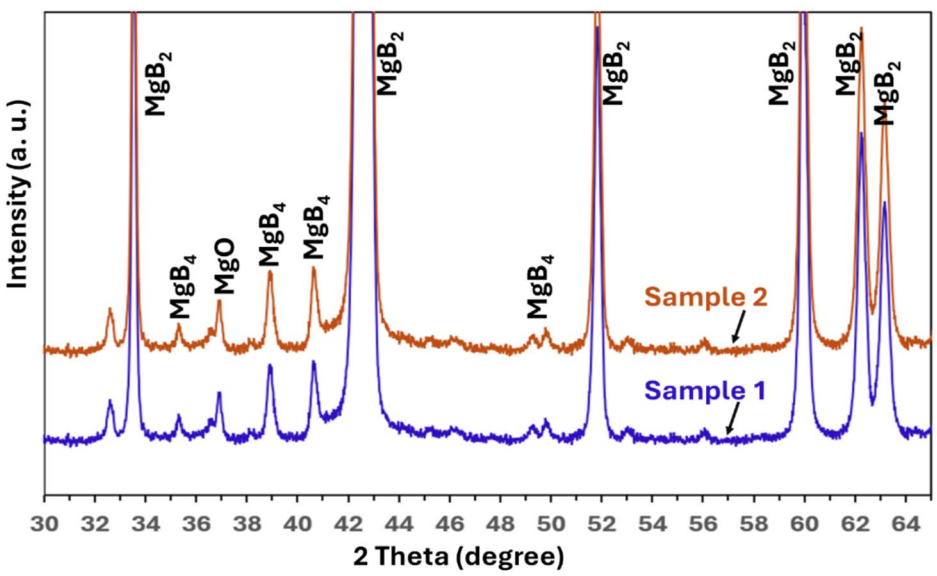

Fig. 6 XRD patterns of MgB_2 bulks sintered at different conditions

4 Conclusion

This work investigates the microstructure of MgB_2 bulk samples in three dimensions using advanced laboratory XCT technique. The MgB_2 samples were prepared by powder processing followed by the FAST sintering process. In addition to the XCT technique, conventional SEM and XRD techniques were also used to examine the microstructure, and a comparison was made between the SEM results (2D analysis) and XCT results (3D analysis). The SEM data, XRD and XCT techniques were found to be complementary for a precise analysis of the microstructure of MgB_2. While the XRD and SEM provide information about the existing phases and the composition, the XCT technique used in this work provides a new insight into the microstructure of the MgB_2 bulks. This includes.

(i) 3D visualization of impurities and defects including pores in MgB_2 which is highly important to understand the connectivity in the MgB_2 matrix in three dimensions and examine the supercurrent path within the MgB_2 superconductor. Our work showed that although the impurity phases and porosity exist in the MgB_2 bulks, there is still a continuous path in the MgB_2 matrix for transport supercurrent.

(ii) The distribution of the impurities and defects in three dimensions which is significant for optimizing the processing conditions including sintering parameters such as pressure, time, and temperature. This information also helps to understand the uniformity of the sample in terms of microstructure and consequently critical current density.

(iii) The 3D visualization of the MgO phase showed that the MgO is in round small particles and is distributed evenly within the MgB_2 matrix. The distribution of the MgO particles was found to be highly affected by the sintering process especially sintering temperature and waiting time before applying the pressure. If the waiting time is longer, larger MgO particles will be formed with larger distances between the particles.

Acknowledgements The use of facilities funded by EPSRC Grant EP/M02833X/1 "University of Oxford: experimental equipment upgrade" is gratefully acknowledged.

Author Contribution Y.W. Data analysis, prepared figures, reviewed the manuscript, wrote some parts of the manuscript. C.G. Advice on sample preparation, Discussion on results. S. S. Discussion on results, Reviewed the paper, Advice on sample preparation. B.S. Advice on data analysis, Reviewed the paper. T.M. Wrote the main manuscript text, Data analysis, Discussion.

Data Availability No datasets were generated or analysed during the current study.

Declarations

Competing Interests The authors declare no competing interests.

References

1. Zhang, Z., MacManus-Driscoll, J., Suo, H., Wang, Q.: "Review of synthesis of high volumetric density, low gravimetric density MgB2 bulk for potential magnetic field applications. Superconductivity **3**, 100015 (2022). https://doi.org/10.1016/j.supcon.2022.100015
2. Mousavi, T., Grovenor, C., Speller, S.: Characterization of superconducting $Fe_y(Se_{1-x}Te_x)$ thin films deposited on MgO substrates by sputtering. J. Mater. Sci. **50**, 6970–6978 (2015)
3. C. Buzea and T. Yamashita, 2001 Review of Superconducting Properties of MgB2. Superconduct. Sci. Technol. 14 https://doi.org/10.1088/0953-2048/14/11/201.
4. Muralidhar, M., Shadab, M., Srikanth, A.S., Jirsa, M., Noudem, J.: Review on high-performance bulk MgB2 superconductors. J. Phys. D Appl. Phys. **57**(5), 053001 (2023)
5. T. Prikhna, V. Sokolovsky, and V. Moshchil, 2024 "Bulk MgB2 Superconducting Materials: Technology, Properties, and Applications," Materials, vol. 17, no. 11, p. 2787, 2024 https://www.mdpi.com/1996-1944/17/11/2787.
6. Putti, M., Grasso, G.: MgB2, a two-gap superconductor for practical applications. MRS Bull. **36**(8), 608–613 (2011). https://doi.org/10.1557/mrs.2011.176
7. Uglietti, D.: A review of commercial high temperature superconducting materials for large magnets: from wires and tapes to cables and conductors. Supercond Sci Technol **32**(5), 053001 (2019). https://doi.org/10.1088/1361-6668/ab06a2
8. Rafieazad, M., Balcı, Ö., Acar, S., Somer, M.: Review on magnesium diboride (MgB2) as excellent superconductor: Effects of the production techniques on the superconducting properties. J. Boron **2**(2), 87–96 (2017)
9. Durrell, J.H., et al.: Bulk superconductors: a roadmap to applications. Supercond. Sci. Technol. **31**(10), 103501 (2018). https://doi.org/10.1088/1361-6668/aad7ce
10. Matthews, G.A.B., Mousavi, T., Santra, S., Grovenor, C.R.M., Grant, P.S., Speller, S.: Improving the connectivity of MgB2 bulk superconductors by a novel liquid phase sintering process. Supercond. Sci. Technol. **35**(6), 065005 (2022). https://doi.org/10.1088/1361-6668/ac5164
11. Y. Meng et al., 2022 Boron-Magnet Nanoparticles Capture Lipopolysaccharide and Peptidoglycan for Bacteria-Infected Wound Healing
12. Mousavi, T., Santra, S., Melhem, Z., Speller, S., Grovenor, C.: Superconducting joint structures for Bi-2212 wires using a

powder-in-tube technique. IEEE Trans. Appl. Supercond. **31**(5), 1–4 (2021)
13. Cai, Q., Ma, Z., Zhao, Q., Liu, Y.: Observation of Flux Jump in $(MgB_2)_{0.96}Ni_{0.04}$ Superconductor Doped with Milled Ni powders. J. Superconduct. Nov. Magn. **24**(6), 2013–2017 (2011)
14. de Castro Sene, F.C.: Review on the state-of-the-art and challenges in the MgB2 component manufacturing for superconducting applications. Superconductivity **9**, 100083 (2023)
15. Serquis, A., et al.: Hot Isostatic Pressing of Powder in Tube MgB2 Wires. Appl. Phys. Lett. **82**, 2847–9 (2003). https://doi.org/10.1063/1.1571231
16. D. Gajda et al., 2016 Experimental research of high field pinning centers in 2% C doped MgB2 wires at 20 K and 25 K. J Appl Phys vol. 120(11) https://doi.org/10.1063/1.4962399
17. Prikhna, T.A., et al.: Peculiarities of high-pressure and hot-pressing manufacture of MgB2-based blocks with high critical currents for electrical machines. J Phys Conf Ser **97**(1), 012022 (2008). https://doi.org/10.1088/1742-6596/97/1/012022
18. Gajda, G., Filar, K., Morawski, A., Diduszko, R., Czujko, T., Gajda, D.: Impact of rare earth oxides metal (Dy, Tb, Er, Eu, Sm) admixtures on the structure, morphology, pinning centers and critical parameters of MgB2 materials manufactured by ambient pressure sintering and hot isostatic pressure processes. Ceramics Int **49**(22), 36031–36043 (2013). https://doi.org/10.1016/j.ceramint.2023.08.283
19. Senatore, C., Hossain, S., Flükiger, R.: Enhanced Connectivity and Percolation in Binary and Doped In Situ MgB2 Wires After Cold High Pressure Densification. IEEE Trans. Appl. Superconduct. **21**, 2680–2685 (2011). https://doi.org/10.1109/TASC.2010.2096376
20. Flukiger, R., Hossain, M.S.A., Senatore, C., Buta, F., Rindfleisch, M.: A New Generation of In Situ MgB2 Wires With Improved J_c and B_irr Values Obtained by Cold Densification (CHPD). IEEE Trans. Appl. Supercond. **21**(3), 2649–2654 (2011). https://doi.org/10.1109/TASC.2010.2101571
21. Gajda, D., et al.: "The significant influence of packing density of unreacted Mg+2B mixture and heat treatment conditions on some of critical parameters for MgB2/Fe wires. J. Alloys Compounds **889**, 161665 (2021). https://doi.org/10.1016/j.jallcom.2021.161665
22. G. Simon and M. Miryala, 2024 "Impact of doping on MgB2 superconductors: a comprehensive review," J. Alloys Compounds Commun 100023
23. Zhang, H., Li, L., Zhao, Y., Zhang, Y.: The performance improvement of MgB2 prepared by the Mg diffusion method with the MgB4 addition. J Phys Confer Ser **871**(1), 012057 (2017). https://doi.org/10.1088/1742-6596/871/1/012057
24. Shimada, Y., et al.: Microstructural connectivity in sintered ex-situ MgB2 bulk superconductors. J Alloys Compounds **656**, 172–180 (2016). https://doi.org/10.1016/j.jallcom.2015.09.253
25. Dou, S.X., et al.: Enhancement of the critical current density and flux pinning of MgB 2 superconductor by nanoparticle SiC doping. Appl. Phys. Lett. **81**(18), 3419–3421 (2002)
26. Maire, E., Withers, P.J.: Quantitative X-ray tomography. Int. Mater. Rev. **59**(1), 1–43 (2014)
27. Olmos, L., Bouvard, D., Cabezas-Villa, J.L., Lemus-Ruiz, J., Jiménez, O., Arteaga, D.: Analysis of Compression and Permeability Behavior of Porous Ti6Al4V by Computed Microtomography. Met Mater Int **25**(3), 669–682 (2019)
28. Wan, F., Pirzada, T.J., Liu, R., Wang, Y., Zhang, C., Marrow, T.J.: Microstructure Characterization by X-Ray Computed Tomography of C/C-SiC Ceramic Composites Fabricated with Different Carbon Fiber Architectures. Appl Compos Mater **26**(4), 1247–1260 (2019). https://doi.org/10.1007/s10443-019-09778-2
29. Li, Y., Chi, Y., Han, S., Zhao, C., Miao, Y.: Pore-throat structure characterization of carbon fiber reinforced resin matrix composites: Employing Micro-CT and Avizo technique. PLoS ONE **16**(9), e0257640 (2021). https://doi.org/10.1371/journal.pone.0257640
30. Morankar, S., Mandal, M., Kourra, N., Williams, M.A., Mitra, R., Srirangam, P.: X-Ray Tomography Study on Porosity and Particle Size Distribution in In Situ Al-4.5Cu-5TiB2 Semisolid Rolled Composites. JOM **71**(11), 4050–4058 (2019). https://doi.org/10.1007/s11837-019-03385-z
31. Moseley, D.A., Wilkinson, D.P., Mousavi, T., Dennis, A.R., Speller, S., Durrell, J.H.: A new MgB2 bulk ring fabrication technique for use in magnetic shielding or bench-top NMR systems. Supercond. Sci. Technol. **35**(8), 085003 (2022)
32. Zhu, Y., et al.: Microstructure and structural defects in MgB2 superconductor. Physica C **356**(4), 239–253 (2001)